THE ASTRONOMICAL JOURNAL VOLUME 78, NUMBER 10 DECEMBER 1973

The low-frequency spectra of nonthermal radio sources

R. S. Roger
Dominion Radio Astrophysical Observatory, National Research Council, Penticton, B. C. Canada

A. H. Bridle
Astronomy Group, Department of Physics, Queen's University at Kingston, Ontario, Canada

C. H. Costain
Dominion Radio Astrophysical Observatory, National Research Council, Penticton, B. C. Canada

(Received 1 August 1973)

Flux densities of discrete radio sources measured with the 10–22-MHz T-arrays at the Dominion Radio Astrophysical Observatory are combined with observations from higher frequencies to construct and classify the continuum spectra of 225 sources in the range 10–2000 MHz. New or revised flux densities are given for 38 sources at 10 and 22 MHz, together with revised calibration factors for previously published flux densities at these frequencies. Scales used for other published flux densities in the range 12–178 MHz are assessed and an internally consistent set of scale revision factors is derived. The spectral properties of complete samples of extragalactic sources selected at 10, 178, and 1400 MHz are compared, using spectral indices evaluated at six frequencies. Classes of sources having unusually high- and low-spectral indices are identified. Quasistellar sources are found to have spectral indices distributed differently from those of radio galaxies; quasistellar sources with power-law regions of their spectra have generally higher spectral indices there than those of the galaxies. A small group of sources identified with blank fields contains some members whose spectral indices are uncharacteristic of distant radio galaxies or of quasistellar sources. There appears to be no evolutionary effect present in the spectral index–luminosity correlation for radio galaxies.

I. INTRODUCTION

NEARLY all spectral flux-density measurements at wavelengths greater than about 3 m have been made with specialized radiotelescopes operating over a limited frequency range. Because sensitivity is usually less a problem than source confusion, the most economic means of obtaining such measurements is with extensive unfilled apertures of the X or T-array type. The measurements are limited by two factors; the knowledge of the gain of the instrument, often as a function of zenith angle and, especially at the longer wavelengths, the observing conditions imposed by scintillation, refraction, and absorption in the Earth's ionosphere. These latter effects are usually overcome by repeated observations and severe selection of the data.

The determination of radio source spectra from such measurements necessarily consists of accumulating flux densities measured with several different instruments each separately calibrated. This has the somewhat dubious advantage that systematic effects peculiar to only one set of measurements are fairly easily recognized and corrected. Errors due to random effects introduced by the instrument or the ionosphere require that any deviatory trend in a spectrum shown by a flux density at one wavelength needs confirmation by independent measurements before it is convincing.

In 1963–1965 two large T-arrays were constructed at the Dominion Radio Astrophysical Observatory for radio source and galactic background surveys at 10 MHz (Galt, Purton, and Scheuer 1967) and 22 MHz (Costain, Lacey, and Roger 1969). Flux-density measurements resulting from these surveys have been separately published (Bridle and Purton 1968; Roger, Costain, and Lacey 1969). In this paper we report 38 additional or revised flux densities at these frequencies and describe a recalibration of the flux-density scales at both frequencies. These revised flux densities are combined with selected measurements at higher frequencies to construct the spectra of 225 nonthermal radio sources below 2 GHz.

The flux-density scales used by other low-frequency observers, namely the group at the Ukrainian Academy of Sciences at Grakovo and at the University of Maryland's Clark Lake Radio Observatory are compared with ours, but in the construction of the spectra we have deliberately used only our own measurements below 38 MHz since these are the only ones we can defend for individual sources. The flux-density scales of the higher frequency measurements, particularly in the range 38–178 MHz, also require careful evaluation. Large correction factors to the scales used by Conway, Kellermann, and Long (1963) have been proposed (e.g., Scott and Shakeshaft 1971) and in the next two sections we derive scale conversion factors which we consider are mutually consistent from 10 to 178 MHz.

In the other sections we describe individual source spectra, analyze those of three complete samples of sources, and compare the spectra of specific groups of extragalactic sources.

II. THE LOW-FREQUENCY FLUX DENSITIES

A. The 22-MHz Scale

The 22-MHz flux densities are measured with respect to a flux density for Cygnus A of 29 100 f.u. (1 f.u. $= 10^{-26}$ Wm^{-2} Hz^{-1}) (Roger, Costain, and Lacey 1969, hereafter referred to as RCL). There is now general agreement on the flux density of this source in the range 20–40 MHz (Parker 1968; Braude, Lebedeva, Megn, Ryabov, and Zhouck 1969). Recently Viner (1971)

at the Clark Lake Radio Observatory has obtained an absolute measurement of the flux density of Cygnus A at 26.3 MHz. Using a method based on that of Little (1958), he obtains a value of 28 700±1500 f.u., in good agreement with the value assumed above.

The previous scaling of all weaker sources to the flux density of Cygnus A reported in RCL has been found to be in error due to the difference between the true and nominal loss of attenuators inserted in the 22-MHz array for observations of Cas A and Cyg A. The error is confirmed by independent measurements of seven intense sources (Cas A, Cyg A, Vir A, Her A, Tau A, Hyd A, and 3C 123) made with the fan beam of the E–W arm of the 22-MHz array. As a result, all flux densities listed in the RCL catalog, except those of Cas A and Cyg A, have been revised upwards by the factor 1.15. The uncertainty of the scaling with respect to Cygnus A is ±5%.

Considerable care has been taken to ensure the linearity of the flux-density scale over the entire range 30–6000 f.u. (Cas A and Cyg A were attenuated to within this range). Each observation of a discrete source was accompanied by a noise temperature calibration whose magnitude was of the same order as the correlated antenna temperature due to the source. The calibration power derived from a single temperature-limited noise diode was split and added separately through couplers to the coaxial lines feeding each arm of the T antenna to its respective preamplifier (Costain *et al.* 1969). The linearity of the noise power as a function of diode current was verified with precision attenuators and the output power was checked against that from another diode noise source of different manufacture. No deviations from linearity greater than 1% were detected.

Figure 1 shows the mean ratios of the 22-MHz flux densities to those at the same frequency interpolated from the 20 and 25-MHz measurements of the Ukrainian UTR-1 radio telescope at Grakovo (Braude *et al.* 1969; Braude, Lebedeva, Megn, Ryabov, and Zhouck 1970a) for various flux-density ranges. Also shown are the mean ratios of the 22-MHz flux densities to unpublished flux densities at 26.3 MHz from the Clark Lake Radio Observatory (Viner 1971). It can be seen that there is general agreement between all three scales for flux densities greater than 1000 f.u. Furthermore, the agreement between Penticton and Clark Lake scales continues down to at least 50 f.u. However, the ratio of the Grakovo to Penticton scales increases progressively to a value 1.4 at 100 f.u. This disagreement was noted by Braude, Megn, Ryabov, and Zhouck (1970b), and was used by them as a basis for revising the 22-MHz flux densities in RCL to the Grakovo scale. In view of the care taken to ensure the linearity of the 22-MHz scale and of the good agreement of the Penticton scale with the Clark Lake scale down to the 50 f.u. level, there seems to be little justification for such a revision.

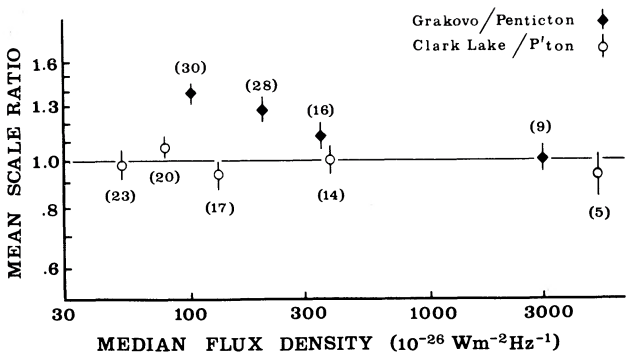

FIG. 1. The mean ratios of flux densities near 22 MHz measured by the Ukrainian Academy of Sciences (Grakovo) to those used in the present study (Penticton); and similar ratios of U. of Maryland (Clark Lake) values to Penticton values. The latter ratios are corrected for the slight frequency difference (26.3–22 MHz). Numbers in parentheses indicate sources in each mean.

B. SUPPLEMENTARY FLUX DENSITIES AT 22-MHZ

Twenty-five flux densities listed in Table I have been added to the revised RCL data for the determination of source spectra. Nineteen of these measurements are entirely new; the other six (marked with asterisks) replace values given in RCL. All flux densities listed in Table I incorporate the correction factor (×1.15) referred to in the preceding section.

C. THE 10-MHZ SCALE

The 10-MHz flux densities used in this paper have been placed on a revised flux-density scale obtained by two methods. The first is that of Bridle and Purton (1968), henceforth referred to as BP, who adopted as a primary standard the 10.05-MHz flux density of Cas A measured on an absolute scale by Bridle (1967) at the mean epoch of their observations. BP calibrated the gain of the 10-MHz telescope at high zenith angles by adjusting the parameters of a theoretical model of the gain-zenith angle dependence to achieve agreement with the extrapolated flux densities of selected sources. We have repeated this procedure using the revised 38, 178, 750, and 1400 MHz scales (Kellermann, Pauliny-Toth, and Williams 1969, and this paper, Sec. III). The resulting revisions to the 10-MHz calibration could be adequately represented by raising by 25% the flux densities of all sources at zenith angles greater than 15°. The second method is based directly on the revised 22-MHz scale (see Sec. IIA). The spectra of twelve sources at $|b|>20°$ which are not known to contain compact structure and whose spectra are well-determined power laws between 22 and 1400 MHz were extrapolated to 10.03 MHz. Comparison of the extrapolated flux densities with those of BP suggested that the latter should be raised by 15%: this correction is of the same order as the rms uncertainty due to nonlinearities in the receivers and to ionospheric effects in calibrating the observations of the weaker BP sources relative to Cas A.

TABLE I. New and revised flux densities at 22 MHz.

Source	Flux density 10^{-26}Wm^{-2}Hz^{-1}	Comments
3C 6.1	71±10	Background uncertain
*3C 29	83 20	Confusion with 4C-00.06 and 4C-01.04
*3C 31	86 13	Confused with 3C 34
3C 34	69 10	Confused with 3C 31
*3C 41	72 17	Confused with 4C 32.07
3C 61.1	125 35	Large beam pointing uncertainty
3C 118, (P 0428+01)	82 20	
0744+55, (DA 240)	123 15	Includes 4C 56.16
4C 55.16, (0831+55)	30 5	
3C 208	68 15	Confused with 3C 208.1
3C 208.1	48 15	Confused with 3C 208
3C 212	30 8	
4C 31.33, (0919+31)	46 8	Includes 4C 31.33
3C 227	205 30	
3C 250	108 20	
3C 273	410 70	Confused with 3C 274 sidelobes
3C 275.1	46 6	
3C 295	67 17	Confused region; other sources not cataloged.
	(128 20)	(Alternative interpretation with source on broad background feature)
*P 1435+038	90 20	Flux density assigned to MSH 14+0/10 in RCL. Confused with P 1434+03
*3C 306.1	80 16	Confused with P 1452–05
3C 313	150 25	Confused with 3C 317
3C 317	310 40	Confused with 3C 313 and 3C 318.1
3C 318.1	295 25	Confused with 3C 313
*3C 337	85 25	Confused with following source, possibly NRAO 508
3C 445	250 55	Confused region

* Entries replace values given in RCL.

We have therefore raised all BP flux densities, except the absolute measurements of Cas A and Cyg A, by a factor of 1.20 whose uncertainty is of order 10%. This correction is in satisfactory agreement with the absolute measurements, with the theoretical model of the antenna response, and with our adopted flux-density scale at 22, 38, 178, 750, and 1400 MHz. The correction is significantly less than that proposed by Braude *et al.* (1970b), who suggested revising the BP flux densities upwards by a factor 1.66±0.25.

Braude *et al.* argued that the aperture efficiency of the 10-MHz telescope had been seriously overestimated. Their analysis, based on their estimate of the efficiency derived from two published records obtained with the instrument, appears to have overlooked two features of its operation that have been described in the literature. The sources discussed by Braude *et al.* do not transit through the maxima of the fixed reception patterns available from the Butler–matrix phasing system of the 10-MHz telescope (Galt *et al.* 1967); furthermore, a 10-sec time constant is used for the observations of strong sources, to monitor ionospheric scintillations (Bridle and Purton 1968), but a 90-sec time constant is used for studies of weaker sources. The records analyzed by Baude *et al.*, if correctly interpreted, contain output rms noise fluctuations of ~45 f.u., which may be compared with the maximum rms value of 60 f.u. quoted by BP. The noise level on the 10-MHz records shows appreciable variation over the sky; the dominant noise component is contributed by the nonthermal background radiation, and is not receiver noise as suggested by Braude *et al.*

Braude *et al.* also note that the proportional uncertainties in the BP flux densities are nearly independent of flux density, and claim that this implies that BP underestimated the effects of receiver noise. They overlook the fact that the dominant uncertainties in the BP data are those introduced by the lack of repeatability of 10-MHz measurements due to changing ionospheric refraction, scintillation, scattering and absorption. These uncertainties are equally serious for sources of all flux densities.

The 10-MHz flux densities for Cas A, Cyg A, 3C 84, 3C 123, 3C 144, and 3C 348, revised as described above, have been compared with those published by Clark (1966) and by Hamilton and Haynes (1968). The mean ratio of our revised 10-MHz flux densities to those of these independent workers is 1.02±0.12. The source 3C 218 was excluded from this comparison because the BP observation is subject to very large ionospheric uncertainties, as noted in their paper.

We have also compared 12.6-MHz flux densities interpolated from the spectra derived in Sec. IV of this paper with those given by Braude *et al.* (1969). The ratio of the flux densities given by Braude *et al.* to our interpolated values is plotted as a function of flux density in Fig. 2. The discrepancy between the Grakovo scale and our own increases with decreasing flux density;

TABLE II. New and revised flux densities at 10 MHz.

Source	Flux density $10^{-26}Wm^{-2}Hz^{-1}$	Comments
4C 39.18	115±35	BP incorrectly identify as 3C 186
*4C 31.33, (0919+31)	105 30	Corrected for confusion with 4C 31.34
3C 238	220 55	Does not include 3C 237
*3C 245	170 40	
3C 247	110 35	
4C 21.33	145 35	BP incorrectly identify as 3C 263.1
3C 286	85 25	
*3C 288	160 50	Corrected for confusion with 4C 39.40 and 4C 38.37
*3C 293	170 35	Corrected for confusion with 4C 32.46
*3C 330	110 60	Corrected for confusion with 4C 65.20
4C 65.20	85 35	
*3C 356	110 30	Corrected for confusion with 4C 50.43
*3C 388	175 85	Corrected for background confusion

* Entries replace values given in BP.

the effect is similar to, but more severe than, that encountered in similar comparisons at 20 MHz (Sec. IIA of this paper), where good agreement was found between the Penticton and Clark Lake Scales. It appears that the Grakovo flux densities of weak sources are systematically overestimated in a way which becomes more pronounced as the observing frequency is decreased.

Additional evidence of this effect can be found by examining the spectra fitted to the Grakovo flux densities by Braude *et al.* (1970b). We consider only those sources classified by them as having power-law (i.e., straight) spectra and compare *their* measured flux densities (Braude *et al.* 1969, 1970a) at each of their observing frequencies (12.6, 14.7, 16.7, and 25 MHz) with those calculated by fitting *their* spectral indices to *their* 20-MHz flux densities. The mean ratio of the measured flux densities to the derived ones is an indication of the relative calibration at each frequency with respect to that at 20 MHz. The mean ratios and their standard errors are:

12.6 MHz	1.29±0.04
14.7 MHz	1.18±0.04
16.7 MHz	1.07±0.03
20.0 MHz	1.00 defined
25.0 MHz	1.16±0.04

A trend which would lead to increasing overestimation of flux densities from 20 to 12.6 MHz is readily apparent. It is emphasized that these ratios are an *underestimation* of the true effect since this discussion excludes all but power-law spectra, in particular, the large proportion of sources classified by Braude *et al.* (1970b) as having excess flux density at low frequencies. Flux densities at 25 MHz also appear to be overestimated with respect to those at 20 MHz.

D. SUPPLEMENTARY FLUX DENSITIES AT 10 MHZ

Thirteen flux densities listed in Table II have been added to the revised BP data for the determination of source spectra. Four of these measurements are entirely new; the other nine (marked with asterisks) replace the values given in BP. All flux densities listed in Table II incorporate the correction factor (×1.20) referred to in the preceding section.

III. HIGHER-FREQUENCY FLUX DENSITIES

For most sources, consideration has been restricted to higher-frequency flux densities contained in recently published lists which are reasonably complete to the 3C flux-density limit. Such lists are referred to as primary data in Table III. The most comprehensive is that of Kellermann, Pauliny-Toth, and Williams (1969) (hereafter referred to as KPW) which gives flux densities at 38 and 178 MHz measured at the Mullard Observatory, Cambridge and at 750, 1400, 2695, and 5000 MHz measured at the NRAO, Green Bank.

KPW refer to the uncertainty of the flux-density scales at 38 and 178 MHz suggested by unpublished measurements of Collins at 81.5 MHz. The scales at 38 and 178 MHz are based on the CKL scale (Conway, Kellermann, and Long 1963). Scott and Shakeshaft (1971) have reported that more recent 81.5-MHz measurements are consistent with the CKL scale for

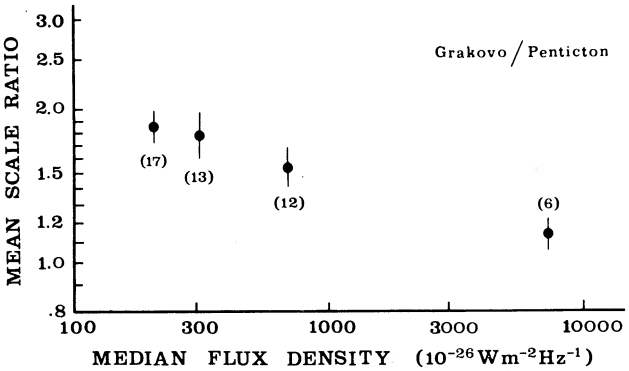

FIG. 2. The mean ratios of flux densities at 12.6 MHz measured by Grakovo Observatory to those interpolated in the present study. Numbers in parentheses indicate number of sources in each mean.

TABLE III. Data used in constructing spectra.

	Frequency (MHz)	Revision factors
Primary data		
Bridle and Purton (1968)	10.03	1.20±.10(S<10000 f.u.)
This paper, Table II	10.03	...
Roger, Costain, and Lacey (1969)	22.25	1.15±.05(S<10000 f.u.)
This paper Table I	22.25	...
Artyukh, Vitkevich, Dagkesamanskii, and Kazhukov (1969)	86	0.94+03
Kellermann, Pauliny-Toth and Williams (1969)	38	1.18±.03(S<550 f.u.)
	178	1.09±.03(S<160 f.u.)
	750, 1400, 2695, 5000	...
Bridle, Davis, Fomalont, and Lequeux (1972)	1400	...
Secondary data		
Williams, Kenderdine, and Baldwin (1966)	38	1.18
Mills, Slee, and Hill (1958)	85	...
4C Catalogues (Pilkington and Scott 1965; Gower, Scott, and Wills 1966)	178	1.09
4C(T) Catalogue (Caswell and Crowther 1969)	178	1.09
Condon (1971)	318	...
Niell (1971)	430, 759, 1400	...
Parkes Catalogues (Shimmins and Day 1968; Staff of Divn of Radiophysics 1969)	408, 635, 1410, 2650	...
Bridle and Davis (1972)	1400	...
Wall, Shimmins, and Merkelijn (1971)	2700	...
Doherty, MacLeod, and Purton (1969)	10600	...
Zimmermann (1970)	10700	...

a few intense sources but that their flux densities less than about 300 f.u. at this frequency are in excess of the CKL scale by 22±5%. There is as yet no complete set of flux densities at 81.5 MHz based on the Scott and Shakeshaft scale. We have used the 86-MHz measurements by Artyukh, Vitkevich, Dagkesamanskii, and Kozhukov (1969, hereafter referred to as AVDK) as primary data. In Table IV we have compared the AVDK scale, which is based on that of Kellermann (1964), with that proposed by Scott and Shakeshaft (abbreviated to SS in the Table) after allowing for the slight frequency difference. We have also compared AVDK flux densities with those measured by Mills, Slee, and Hill (1958) (abbreviated to MSH in the Table). It is clear that there is general agreement between the three scales and that the recent work by Scott and Shakeshaft confirms the original MSH scale based upon the absolute calibration by Little (1958).

We have compared the 38 and 178-MHz scales used by KPW and the 86-MHz scale of AVDK with flux densities interpolated using measurements at 22 MHz (the scale described in the preceding section) and 750, 1400, and 2695 MHz (from KPW). A group of 38 spectra well fitted by a power-law relationship over the entire frequency range was chosen for the comparison. Scale conversion factors derived in this way for the three frequencies are listed in column three of Table III. The error in the determination of these factors does not include the effect of the 5% uncertainty in the revision of the 22-MHz scale from that of RCL. In view of this, the deviation of the 86-MHz factor from unity is probably not significant.

These factors have been applied in our calculations of spectral indices. For calculations of the indices of sources whose high-frequency flux densities are not listed in the primary data, use has been made of secondary lists given in Table III.

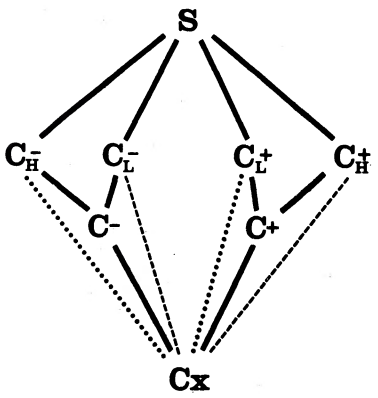

FIG. 3. The hierarchy of complexity used in classifying the spectra. Complexity increases downwards with solid, dashed, and dotted lines indicating combinations of curvature which lead to a spectrum being classified as complex.

TABLE IV. Comparison of flux-density scales near 80 MHz.

Scales	Ratio	s.e.	Number of sources
AVDK/SS	0.96	±0.03	12
AVDK/MSH	1.00	±0.05	35 ($0°<\delta<10°$)
AVDK/MSH	0.88	±0.08	17 ($-6°<\delta<0°$)
AVDK/present work	1.06	±0.03	38

IV. THE SPECTRA

A. Method of Classifying Spectra

We have attempted to fit each spectrum with the simplest curve consistent with the flux densities and their quoted errors; our criterion for simplicity is that of minimum curvature. In general, no trend to a more complex fit is followed unless it is required by two or more measurements. An exception is made for apparently significant trends indicated only by the flux density at the lowest frequency (10 or 22 MHz). Although flux densities observed at frequencies up to 5 and 10 GHz have been considered in assessing the reality of spectral trends, the classifications themselves refer only to the spectra below 2 GHz.

The scheme for classification is as follows:

S Spectral index constant for $\nu < 2$ GHz.

$C-$ Second derivative negative on a plot of $\log S$ versus $\log \nu$.

$C+$ Second derivative positive on a plot of $\log S$ versus $\log \nu$.

C_L- Constant spectral index $\nu > 200$ MHz; remainder
C_L+ of spectrum as above.

C_H- Constant spectral index $\nu < 200$ MHz; remainder
C_H+ as above.

Cx Complex spectrum exhibiting both $C-$ and $C+$ features.

Figure 3 illustrates the hierarchy of complexity.

For a number of sources the spectrum can equally well be classified in two ways. In some such cases further information about the source, such as its structure, might provide a basis for choosing between alternative classifications. We have, however, preferred to retain both alternatives for such sources for two reasons: to indicate where such ambiguities exist in the spectral data taken by themselves, and to avoid biasing the spectral statistics toward any particular theoretical source model.

B. Determination of Spectral Indices

We use the CKL definition of the spectral index α in relating the flux density S to frequency ν, namely,

$$S(\nu) \propto \nu^{-\alpha(\nu)}.$$

It should be noted that this definition produces indices opposite in sign to those of KPW. For each source, a curve is fitted to the data on a $\log S$–$\log \nu$ plot and the slopes of this curve are used to determine the spectral indices at six standard frequencies: 15, 30, 70, 200, 600, and 1800 MHz.

Spectra classified as S have been fitted with straight lines by the method of least squares in which each flux density is weighted inversely to the square of its quoted error. The straight portions of more complex spectra have also been fitted in this way.

For the remaining spectra, a curve was drawn through the $\log S$–$\log \nu$ plot by eye and the flux densities on the curve were read at the n frequencies of the primary catalogs. The curve was then reconstructed as a polynomial of degree n and the spectral indices at the six standard frequencies were determined from the derivative of this polynomial. We prefer this empirical approach to more formal curve fitting as the analytic forms of most curved spectra are unknown. Exceptions are the spectra of those sources at low galactic latitudes which show evidence of interstellar free–free absorption; the indices given for these sources correspond to the form of the absorption cutoff imposed by a uniform medium. Similarly, the indices of sources with high-brightness temperatures, and whose spectra are consistent with a simple synchrotron self-absorption cutoff, are calculated from the analytic expression for such self-absorption. The use of a simple self-absorption fit presupposes that the source is homogeneous and for this reason is less justified than the galactic free–free absorption fit.

C. The Table of Spectral Indices

Table V lists spectral indices for 226 sources. The source designations are given in Column 1. The symbols * † and ‡ designate members of statistically complete samples which are described in the next section.

Columns 2 and 3 list the galactic coordinates of each source. Column 4 gives its optical identification using the following code:

G radio galaxies without bright nuclei, or of undetermined type.

N, db galaxies with bright nuclei, other than Seyfert galaxies; from the list of Burbidge (1970).

SEY Seyfert Galaxies.

Q quasistellar objects.

SNR supernova remnants.

Axxx significant association with Abell Cluster xxx (Abell, 1958) on the Wills (1966) criterion.

? doubtful identification.

Obsc obscuration present.

□ blank field on Palomar Sky Survey prints, no obscuration.

Column 5 lists the spectral classification of the source as described in the preceding section. Alternative classifications are given in the order of increasing complexity unless the more complex classification was supported by a trend involving three or more data points. Marginal alternatives are bracketed. An element of subjectivity is inevitable in deciding on classification order and bracketing in marginal cases. Columns 6–11 give the spectral indices corresponding to that classification at the six standard frequencies. In general, the second decimal place in a spectral index is significant only for the S classifications. It has, however, been retained for most curved fits to indicate the trend

TABLE V. Spectral indices.

(1) Source	(2) l	(3) b	(4) Id	(5) Spectral class	(6) α_{15}	(7) α_{30}	(8) α_{70}	(9) α_{200}	(10) α_{600}	(11) α_{1800}	(12) Comments	(13) Notes
					Spectral indices							
3C 2	99	−61	Q	S				0.72				
*3C 6.1	121	17	?	C−		0.54	0.62	0.77	0.82	0.86		a
3C 9	112	−47	Q	C−	0.63	0.79	0.92	0.96	1.05	1.05		
3C 10, [Tycho SNR]	120	1	SNR	Cx	−0.6	0.50	0.80	0.77	0.61	0.57	FFA(τ_{20}=0.39±0.15)	
‡3C 15	115	−64	G	C−		0.45	0.57	0.68	0.71	0.78		d7
3C 16	118	−49	□	S				0.91				d7
‡*3C 17	115	−65	N	C_L+		1.5	0.83	0.62	0.62	0.62		
3C 19	120	−30	□	S	(<0.7)			0.74				
‡*3C 18	119	−53	G	S				0.73			S_{86} high	
3C 20	122	−11	G	C_H−	0.61	0.61	0.61	0.61	0.69	0.72		d8
3C 22	123	−12	Q?	S				0.85			S_{22} low	
3C 27	123	5	Obsc	C_H−	0.62	0.62	0.62	0.62	0.64	0.76		
3C 28	124	−36	G(A115)	S				1.10				
‡*3C 29	126	−64	G	S				0.66				a
†‡3C 31	127	−30	G	Cx	(0.83)	0.83	0.83	0.79	0.33	0.66		a, d2–3, ⊙
‡*3C 33	129	−49	G	S				0.72				
3C 34	128	−31	□?	S				0.89			S_{38} high	a, d3, i, ⊙
3C 35	126	−13	G	S				0.89			S_{22} low	g, ⊙
‡*3C 40	142	−63	G(A194)	Cx		1.3	1.0	0.75	0.67	0.9		⊙, d2–4, h
3C 41	131	−29	G?	S				0.70			S_{96}, S_{178} low	
				(Cx)		1.0	0.93	0.52	0.59	0.70		
3C 43	134	−39	Q	S				0.76			good fit	
3C 46	132	−24	G	S				1.02				f
†*3C 47	137	−41	Q	C_L−	0.4	0.95	1.00	1.00	1.00	1.00		
3C 54	135	−18	?	S				0.87				
†*3C 55	140	−32	Q?	C_L−	0.4	0.92	0.97	0.97	0.97	0.97	S_{1400} low	
				S				0.94			S_{10}, S_{1400} low, S_{178} high	
*3C 61.1	125	24	G?	C−		0.58	0.69	0.76	0.87	0.91		a
*3C 63	167	−57	G	C_L−		0.4	0.90	0.94	0.94	0.94		
				S				0.88			S_{22} low	
3C 64, P 0219+08	158	−48	G	S				0.76				
†‡*3C 66	140	−17	G(A347)	Cx	0.5	1.61	0.84	0.63	0.63	0.66		
†3C 65	142	−20	□	C_H−	0.83	0.83	0.83	0.83	0.83	0.99	S_{86} high. S_{178}(4C) fitted	
3C 68.1	146	−24	□	S				0.85			S_{86} high.	
†3C 68.2	147	−26	□?	C_L−	0.70	0.95	1.08	1.30	1.30	1.30		
†4C 28.06, (0232+28)	149	−28	G?	S				0.99				d5–6, i
3C 69	136	− 1	Obsc	C_L−	(0.6)	0.92	0.92	0.92	0.92	0.92	FFA($\tau_{20}\leq$0.24). Steepens above 2 GHz	d7
P 0235–19	201	−65	□	S				0.83				c, d1
‡3C 71, [NGC 1068]	172	−52	SEY	Cx		1.03	0.59	0.54	0.61	0.76		
				(S)				0.67				
3C 73, (0247+39)	147	−18		S				0.88			S_{178}(4C) low (resolved)	h
‡*3C 75	170	−45	db (A400)	Cx	1.2	1.1	0.8	0.7	0.7	0.8	S_{38} high	d2–4
				S				0.77			S_{86}, S_{178} low	
†0258+35	151	−20	G(A407)	S				0.97				i, ⊙
‡*3C 78	175	−45	G	S				0.58			S_{178} low	d2–4
				(C+)		0.65	0.65	0.58	0.52	0.52		
‡*3C 79	164	−34	N	C−	0.63	0.63	0.63	0.78	0.98	0.98		d2–4–7
3C 84, Per A[NGC 1275]	151	−13	SEY (A426)	Cx	1.0	1.42	10.6	0.92	0.75	0.53		
3C 86	144	− 1	Obsc	C_L−		0.2	0.6	0.67	0.67	0.67	FFA(τ_{20}=0.48±0.17)	⊙

TABLE V (*continued*)

(1) Source	(2) l	(3) b	(4) Id	(5) Spectral class	(6) α_{15}	(7) α_{21}	(8) α_{70}	(9) α_{200}	(10) α_{600}	(11) α_{1800}	(12) Comments	(13) Notes
					Spectral indices							
‡*3C 88	181	−42	G	S				0.70				
4C 55.07, (0328+55)	144	− 0		S			1.3				Fit to S_{22}, S_{38}, S_{178} only	
*3C 89	186	−43	G	S			1.03					
‡*3C 98	180	−31	G	Cx	0.1	0.94	0.88	0.79	0.74	0.64		
3C 103	157	− 7	?	C−	0.3	0.72	0.82	0.84	0.84	0.95	FFA(τ_{20}=0.15±0.09)	
‡*3C 105	188	−34	□	S				0.67				
P 0405−12	205	−42	Q	C+		1.10	1.02	0.94	0.79	0.50		c
‡*3C 109	182	−28	N	S			0.81					
3C 111	162	− 9	Obsc	Cx	0.4	0.70	0.78	0.80	0.72	0.58	FFA(τ_{20}=0.12±0.06)	
3C 118 (P0428+01)	194	−30		S				0.92			S_{38} low	
3C 123	171	−12	G	C_L−	0.2	0.6	0.72	0.74	0.74	0.74	FFA(τ_{20}=0.15±0.07). Steepens above 2 GHz	d7
3C 130	155	5	G	S			0.85					
				C_L−	0.5	0.8	0.86	0.87	0.87	0.87	FFA($\tau_{20}\leq$0.24)	
3C 131	171	− 8	Obsc	Cx	1.8	1.35	0.85	0.83	0.79	0.88		d7
3C 132	179	−13	G	C_L−		0.25	0.73	0.81	0.81	0.81	FFA(τ_{20}=0.64±0.30) Steepens above 2 GHz	d7
												⊙
HB 9, (0457+46)	153	8	SNR	S			0.46					
3C 133	178	−10	Obsc	C_L−	0.3	0.6	0.69	0.72	0.72	0.72	FFA?($\tau_{20}\leq$0.24)	j
3C 134	168	− 2	Obsc	C−	0.3	0.83	0.97	1.00	1.00	1.08	FFA(τ_{20}=0.19±0.08)	
3C 136.1	180	− 8	G	C+		1.00	0.99	0.86	0.76	0.64		
3C 141	175	− 1	Obsc	C_L−		0.3	0.88	1.00	1.00	1.00	FFA(τ_{20}=0.80±0.25)	
3C 142.1	198	−14.5	?	C_L−		0.4	0.87	0.91	0.91	0.91	FFA(τ_{20}=0.80±0.30) Steepens above 4 GHz	d7, ⊙
3C 144, Tau A	185	− 6	SNR	C_L+	0.82	0.54	0.31	0.25	0.25	0.25		
3C 154	186	4	Obsc	C_L−	−0.1	0.59	0.76	0.78	0.78	0.78	FFA(τ_{20}=0.22±0.13) Flattens above 2 GHz	
												i, ⊙
0611+42	171	12		S				0.91				
3C 157, [IC 443]	189	3	SNR	C_L−	0.0	0.28	0.36	0.38	0.38	0.38	FFA(τ_{20}=0.12±0.06) Much scatter	
3C 158	197	0	Q?	S			0.98					
3C 161, (0624−05)	215	− 8	□	C_H−		0.65	0.65	0.65	0.65	0.78		
3C 165	191	9	□?	C_H−		0.78	0.78	0.78	0.79	1.03		
3C 166	193	8	G	Cx	0.3	0.6	0.9	1.00	0.85	0.70	S_{10} included	d7
				Cx		0.3	1.12	1.00	0.85	0.70	FFA($\tau_{20}\leq$1.50) S_{10} not included	
*3C 171	162	22	N	C−		0.61	0.70	0.81	0.83	0.83		
3C 173	179	18	Q?	C_H−		0.78	0.78	0.78	0.78	0.98	S_{38} low	
3C 172	191	13	?	C−	0.67	0.68	0.71	0.79	0.86	0.89	S_{86} low	d7
				C_H−	0.80	0.80	0.80	0.80	0.80	0.89	S_{86} low	
3C 175	205	10	Q	C_L−	0.5	0.87	0.95	1.00	1.00	1.00	FFA?($\tau_{20}\leq$0.24) S_{86} low	j
				(S)			0.97				S_{10}, S_{86} low	
3C 180	219	7	G	S			0.85				Good fit	d1
†P 0726+24, 4C 24.15	194	19		S			1.50				S_{38} high	d5–6
3C 184.1	134	29	G	S			0.73				S_{86} high	
†P 0736+21, 4C 21.23	199	20	?	S			1.15				S_{178} low	c, d5–6
3C 186	182	26	Q	C_L−		−0.1	1.00	1.12	1.12	1.12	SSA (ν_m=31±2)	b
3C 187	217	13	G?	S				1.05			S_{178} (3Cr) fitted; 4CT low	e
††*0744+55 (DA 240)	162	30	G	S			0.77					g, ⊙
0755+37 (4C 37.21) NRAO 276/277	183	29		S			0.6				S_{178}(4C) resolved and lobe-shifted	d5–6, h

TABLE V (*continued*)

(1)	(2)	(3)	(4)	(5)	(6)	(7)	(8)	(9)	(10)	(11)	(12)	(13)
					Spectral indices							
Source	l	b	Id	Spectral class	α_{15}	α_{30}	α_{70}	α_{200}	α_{600}	α_{1800}	Comments	Notes
3C 190	208	22	Q?	S			0.85					⊙
3C 191	212	21	Q	S			0.99					
††*3C 192	198	26	G	S			0.77					
††*3C 196	171	33	Q	C−	0.53	0.60	0.67	0.76	0.81	0.86		
*3C 196.1	226	17	G	S				1.14				
3C 198	218	23	G	Cx	0.8	1.9	0.8	1.2	0.9	1.2		
				S			1.0				S_{22}, S_{178} high, S_{38} low	
3C 200	194	33	G	S			0.90					
P 0830+11, 4C 11.28	214	28	Q?	S			1.05				S_{178} (4CT) low	c
‡4C 55.16 (0831+55)	162	37		Cx		0.7	0.6	1.2	−0.1	0.2		
				S				0.30			S_{178} (4CT) low	
P 0832+14, 4C 14.27	211	29	□	Cx		1.4	0.8	0.8	1.34	1.34		c
3C 205	159	37	Q	C_H−	0.87	0.87	0.87	0.87	0.87	0.99	S_{86} high	
†4C 29.31, (0840+29)	194	36	Q	C+	1.45	1.41	1.26	1.05	0.74			d5–6
*3C 208	214	33	Q	C_L−		0.2	0.7	1.09	1.09	1.09		a, j
3C 208.1	214	34	□	S				0.73			S_{86} high	a
P 0854+09, 4C 09.32	220	32	?	C_L+	2.2	1.4	0.98	0.98	0.98	0.98		d1, c
3C 210	198	39	□	S				0.89			May steepen above 3 GHz	
3C 212	214	35	N	C_L−		−0.2	0.5	0.85	0.85	0.85		a, j
3C 215	212	37	Q	C_L−	0.75	0.75	0.85	1.02	1.02	1.02		
*3C 216	178	43	Q	Cx	<0.2	0.75	0.88	0.88	0.81	0.71	SSA(ν_m=17±5). S_{38} low	
0907+18	211	38		S			0.9					c, i, ⊙
†4C 38.27, [0908+38)	185	43		S			1.1					⊙
3C 218, Hyd A,P 0915–11	243	25	db	S				1.00				⊙
††*3C 219	174	45	G	C_H−	0.76	0.76	0.76	0.76	0.80	0.91		f
4C 31.33 (0919+31)	195	45		S		0.93						a, b, i, ⊙
P 0922+14, 4C 14.31	217	41	Q	S			1.15				S_{38} low	c
‡*3C 225	220	44	?	C_L−	0.3	0.4	0.6	0.95	0.95	0.95	S_{38} low	d2–4, f
‡*3C 227	229	42	N	S				0.81				g, ⊙
*3C 228	220	46	G?	S			0.82				S_{38} low, S_{178} high	
3C 230	238	39	?	S				0.86				⊙
‡3C 231, [M 82]	141	41	G Irr	C_H−		0.36	0.36	0.36	0.36	0.47		
††*3C 234	200	53	N	S			0.91				good fit	
1003+35	190	54		S			0.6					g, ⊙
‡*3C 237	232	47	G?	C−		−0.2	0.2	0.55	0.72	0.83		k
3C 238	234	47	□	C_H−	0.88	0.88	0.88	0.88	0.88	1.04	S_{38} low	
3C 239	170	53	G	C−	≤0.45	0.70	0.91	0.97	1.15	1.17		
4C 31.35, (1017+31)	196	57	G?	S				1.04				i
3C 242, P 1022+20	217	56	□	S				0.99				c, d5–6
3C 243, P 1023+06	237	50	□?	S				1.2			Much scatter	c, d1–4, ⊙
†*3C 244.1	151	51	G	C−	0.84	0.84	0.86	0.92	0.94	0.94		d7
3C 245	233	56	Q	S			0.73					b
3C 247	171	62	G?	Cx	1.2	1.2	0.4	0.85	0.88	9.88	SSA(ν_m=170±30)	⊙, k
3C 249	256	51	□	C−		0.38	0.64	0.83	0.95	1.08		
*3C 250	213	67	?	S			1.10				S_{2695} low	
3C 252	185	67	?	C_L−	0.4	1.08	1.14	1.14	1.14	1.14	SSA?(ν_m=13±3)	k
†*3C 254	173	66	Q	C_L−	0.4	0.95	1.01	1.01	1.01	1.01	S_{38} low, SSA(ν_m=12.5±2)	j, k
3C 256	218	69	G?	C_L−		0.0	0.95	1.00	1.00	1.00	SSA(ν_m=29±3)	k
4C 23.28, (1139+23)	223	74	G	S				1.0				⊙
P 1140+21, 4C 21.33	229	73	□	S			0.95					b, d5–6
*3C 263.1	227	74	G?	C−		(−2.0)	0.43	0.74	0.95	1.02	SSA(ν_m=53±5)	b, k, ⊙

TABLE V (*continued*)

(1)	(2)	(3)	(4)	(5)	(6)	(7)	(8)	(9)	(10)	(11)	(12)	(13)
					Spectral indices							
Source	l	b	Id	Spectral class	α_{15}	α_{30}	α_{70}	α_{200}	α_{600}	α_{1800}	Comments	Notes
‡*3C 264 [NGC 3862]	236	73	G(A1367)	Cx	1.2	1.8	0.87	0.80	0.80	0.80		
*3C 265	192	75	G	C−	<0.4	0.71	0.97	0.97	0.97	1.00		k
†1152+55	139	60		S			0.8					h, ⊙
*3C 268.1	128	44	□	S			0.66					
P 1215+03	282	65	G?	S				0.93				c, d1, h, ⊙
‡*3C 270	282	67	G	S				0.58			S_{86} low	
3C 270.1	167	81	Q	C−		0.61	0.71	0.77	0.85	0.90	S_{38} low	d7, k
3C 272	141	74	?	C−		0.3	0.61	0.83	0.99	1.09	S_{38} low	f
‡*3C 273	290	64	Q	Cx		0.6	0.90	0.58	0.18	0.04		a, c, ⊙
‡*3C 274, Vir A [M 87]	284	74	G	S			0.79					
*3C 275.1	293	79	Q	C_L−		−0.3	0.8	0.85	0.85	0.85	SSA ($\nu_m = 34 \pm 4$)	a, d2–4, k
4C 47.35, (1249+47)	123	70		S				0.93				
†Coma C, 1257+28	50	88	A1656	S			1.31				$S_{81.5}$ low (see note)	⊙
††‡*3C 280	120	70	□	C_H−	0.78	0.78	0.78	0.78	0.78	0.82		d7
†1304+46	115	71	A1682	C_L−	0.6	2.1	(2.1)					
3C 284	38	86	G	S			0.90					
				C_L−	0.6	0.90	0.93	0.93	0.93	0.93		
3C 285	103	73	G	S				0.81				
‡*3C 286	57	81	Q	Cx	0.6	0.5	0.3	0.1	0.4	0.51		b, d2–3, ⊙
3C 287.1	326	63	N	C+		0.92	0.92	0.82	0.60	0.55	S_{178}(4CT) low, S_{178} (3Cr) high	e
*3C 288	86	75	G	C−	0.63	0.63	0.63	0.77	0.88	0.97		b
‡3C 293	55	76	G	S			0.66				S_{178}(4C) low	b, d7
				Cx	0.76	0.76	0.76	0.65	0.52	0.70		
‡*3C 295	97	61	G	C−		−0.9	0.10	0.54	0.70	0.91		a
1407±31	52	72	□	S			0.8					d3, h, ⊙
4C 48.38, (1414+48)	90	63		S		1.07						⊙
‡*3C 298	352	61	Q	C−		0.42	0.71	0.95	1.09	1.09	S_{38} low	c, ⊙
				Cx		1.4	−0.6	1.00	1.09	1.09	SSA ($\nu_m = 100 \pm 10$)	
*3C 300	18	68	G	S			0.86				good fit	
†4C 38.39, (1424+38)	67	67	A1914	C_L−	0.6	1.4	(1.7)	(1.7)	(1.7)			⊙
P 1435+038	354	55	G	S				1.16				i, ⊙
3C 306.1	351	47	G	S				0.87			S_{86} high	a
*3C 309.1	110	42	Q	C−		0.23	0.35	0.52	0.56	0.56	S_{86} high	d7
††‡*3C 310	39	60	db	C−	0.81	0.87	0.87	0.94	1.01	1.33		
*3C 313	9	52	G	S				0.91			S_{86} high	a, f
3C 314.1	108	42	G	C_H−		0.98	0.98	0.98	0.98	1.10		
†*3C 315	39	58	db	S			0.85					
‡*3C 317	9	50	G(A2052)	C−		0.81	0.87	0.93	1.14	1.38		a
3C 318	30	55	G	C−		0.28	0.54	0.72	0.82	0.92		k
3C 318.1	11	49	Q?	C_H−		1.6	1.6	1.6	2.14			a, d2–4
3C 319	88	51	G	C−	0.72	0.78	0.78	0.82	0.94	1.02		
3C 320	57	55	G	C_H−		0.81	0.81	0.81	0.87	0.94		
†*3C 321	37	54	□	S			0.82				S_{178}(3Cr,4C) low	
3C 322	89	49	□	C_H−	0.83	0.83	0.83	0.83	0.84	0.98		
‡*3C 327	12	38	G	S				0.87			S_{178}(3Cr,4CT) low	
‡*3C 327.1	12	37	G?	S				0.94				
1602+44	70	48		S			0.96					i, ⊙
‡*3C 330	99	41	□	C_L−	0.15	0.36	0.62	0.78	0.78	0.78		
†4C 35.40, (1615+35)	56	46	G	S			0.86				S_{178}(4C) low (resolved)	d5, h
3C 334	33	41	Q	Cx		0.3	1.3	1.03	0.75	0.77		⊙

TABLE V (*Continued*)

(1)	(2)	(3)	(4)	(5)	(6)	(7)	(8)	(9)	(10)	(11)	(12)	(1e)
					Spectral indices							
Source	l	b	Id	Spectral class	α_{15}	α_{30}	α_{70}	α_{200}	α_{600}	α_{1800}	Comments	Notes
3C 336	41	42	Q	S			0.85				Steepens above 3 GHz	
†*3C 338, [NGC 6166]	63	44	G(A2199)	C−	0.3	0.76	0.93	1.12	1.33	1.56		
3C 337	69	44	G?	S				0.82			S_{38} low. S_{178}(4CT) resolved	a, b, e, ⊙
‡*3C 348, Her A	23	29	G	S			1.01				good fit	
3C 351	90	36	Q	C_L−		0.3	0.72	0.75	0.75	0.75	May steepen above 2 GHz	
3C 352	72	36	□	C_L−		0.1	0.81	1.00	1.00	1.00		
‡*3C 353	21	20	G	S			0.72				S_{86} low	
3C 356	78	34	?	C_L−	0.3	0.5	0.93	1.05	1.05	1.05	S_{22} low	b
3C 357	56	31	G	S				0.73				
3C 368	38	15	Obsc	C−		0.90	1.05	1.16	1.21	1.28		
4C 48.45, (1806+48)	76	27		S		1.0						⊙
‡*3C 380	77	24	Q	Cx	−0.8	0.70	0.87	0.79	0.73	0.57		j
‡*3C 382	61	17	G	S				0.76			S_{178}(4CT,3Cr) low	
3C 386	47	11	G	S				0.70				
‡*3C 388	75	20	G	C−	0.59	0.62	0.66	0.67	0.77	0.86		b
*3C 390.3	111	27	N	S				0.75				
3C 394	45	4	Obsc	S				0.89			S_{86} low	
3C 399.1	63	9	Obsc	C−		0.5	0.6	0.71	0.78	0.82	FFA?($\tau_{20} \leq 0.80$)	⊙
‡*3C 401	93	18	G	C−		0.23	0.46	0.66	0.77	0.87		
3C 402	83	13	G	Cx		1.14	0.97	0.72	0.58	0.78	Fit to S_{178}(4CT)	e
				(S)				0.82			Fit to S_{178}(3Cr)	
3C 405, Cyg A	76	6	G	C−	−0.5	0.4	0.60	0.65	0.88	1.07	FFA($\tau_{20}=0.30\pm0.09$)	
3C 409	63	−6	Obsc	C−	0.3	0.75	0.87	0.89	0.89	1.13	FFA($\tau_{20}=0.17\pm0.08$)	
3C 410	69	−4	Obsc	S				0.65			Steepens above 2 GHz	d7
3C 415.2	90	8	?	S				1.00				
3C 422, P 2044–02	45	−27	G	S				0.77			Much scatter. S_{750} low	c
Cygnus Loop, (2047+30)	74	−8	SNR	S			0.40					⊙
3C 424	54	−22	G	S				0.93				
*3C 427.1	111	19	?	C_L−		0.72	0.86	1.00	1.00	1.00		d7
3C 430	100	8	G	Cx	0.2	0.78	0.89	0.83	0.74	0.70	FFA($\tau_{20}=0.19\pm0.08$) S_{86} low	
3C 432	68	−23	Q	C_L−		0.70	0.95	1.02	1.02	1.02	Steepens above 3 GHz	
‡*3C 433	74	−18	db	C−		0.2	0.71	0.76	0.81	0.88		d7
*3C 436	80	−19	G	S				0.87				
3C 438	89	−13	?	C−	−0.1	0.6	0.76	0.83	0.93	1.07	FFA($\tau_{20}=0.24\pm0.10$)	
3C 441	85	−21	□?	C_L−		0.3	0.83	0.83	0.83	0.83		
				S				0.77			S_{86} high	
*3C 442	75	−34	db	S				0.96			May steepen above 3 GHz	
3C 444, P 2211–17	40	−52	G	S				1.06				c
‡*3C 445	62	−47	N	C+		1.21	1.08	0.84	0.77	0.77		a
3C 446, P 2223–05	59	−49	Q	C+		0.95	0.83	0.58	0.43	0.39		
‡*3C 452	98	−17	G	C−	0.42	0.73	0.84	0.84	0.84	0.90		f
3C 454.1	114	11	□	C_H−		0.97	0.97	0.97	0.97	1.20		
3C 454.2	111	5	Obsc	C+		1.5	1.25	0.97	0.79	0.79	Fit to S_{178}(3Cr); S_{178}(4CT) low	e
‡*3C 459	83	−51	N	C_L−		0.2	0.91	0.95	0.95	0.95	SSA?($\nu_m=27\pm4$). S_{38} low	
3C 461, Cas A	112	−2	SNR	C_L−	−0.4	0.5	0.71	0.76	0.76	0.76	FFA($\tau_{20}=0.32\pm0.06$) S_{22} slightly high	
‡*3C 465	103	−33	A2634	S			0.82				good fit	
3C 470	113	−18	G	C_H−		0.79	0.79	0.79	0.86	0.91	S_{86} low	

* Included in 178-MHz Sample † Included in 10-MHz Sample ‡ Included in 1400-MHz Sample

Notes to TABLE V (*continued*)

3C 298	The synchrontron self-absorption fit applies to the higher frequency component.
4C 38.39	The listed fit is to S_{10}, S_{38}, S_{178}, and S_{1417} from Olsen (1967). In the latter two measurements, the source may be partially resolved.
1435+03	Confused with a smaller source, 1434+03 at 22 MHz. The listed fit is to S_{22}, S_{1400} (BD), and S_{2700} (Wall, Shimmins, and Merkelijn (1435+038).
1602+44	This source includes 4C 44.27 which comprises 75% of flux density at 1400 MHz (BD). The listed fit is to S_{10}, S_{38}, and S_{1400} (total).
3C 334	All low-frequency measurements may be affected by complexity of the galactic background in the neighborhood.
3C 337	This spectrum may include a contribution from NRAO 508 at low frequencies.
4C 48.45	The listed fit is to S_{10}, S_{38}, and S_{178}.
3C 399.1	It is difficult to assess how much of the low-frequency curvature in this spectrum is due to free–free absorption.
3C 405	The listed fit is to the same high-frequency data as used by KPW.
Cygnus Loop	Flux densities at 178 MHz and 960 MHz from Howard and Maran (1965) and at 38 MHz from Kenderdine (1963).

apparent in the log S–log ν plot. Where the index is changing rapidly and the retention of the second decimal place would seriously misrepresent the accuracy with which the index is determined, as is the case near the maxima of absorption cutoffs, only one decimal is listed. Where 22 MHz is the lowest frequency at which measurements have been made, there is no entry in the 15-MHz column. Similarly, where flux densities at higher frequencies are not available, the corresponding indices are absent.

Column 12 contains comments relating to the type of fit, the deviations of specific flux densities from that fit and trends in the spectrum at frequencies above 2 GHz. The abbreviations FFA and SSA indicate the probable presence of interstellar free–free absorption or synchrotron self-absorption, respectively. In such cases the parameters of these analytic fits to the spectra are listed in terms of the optical depth, τ, at 20 MHz (FFA) or the frequency of maximum flux density, ν_m (SSA). Column 13 indicates notes following the Table which apply to that source. Specific notes on individual sources are denoted by the symbol ⊙.

V. SPECTRA OF THREE COMPLETE SAMPLES OF EXTRAGALACTIC SOURCES

A. Choice of the Samples

Three samples of sources have been selected from those listed in Table V for study of their classification and spectral properties. The samples are chosen to be essentially complete to given flux-density limits at each of the frequencies 10, 178, and 1400 MHz.

The need to consider complete samples when discussing statistical properties of sources has been stressed by several authors (Williams and Bridle 1967; Kellermann, Pauliny-Toth, and Davis 1968; van der Laan 1969). It is well understood that the choice of observing frequency biases the content of samples complete to any given flux-density limit; the sources listed in Table V are indeed only those with sufficient emission to be observed at long wavelengths.

The 10-MHz sample is selected from the survey data of Bridle and Purton (1968) and contains 30 sources in a region of sky bounded by $20°<\delta<60°$, $0^h<\alpha<16^h30^m$, and $|b|>15°$. The sample is complete to a (revised) 10-MHz flux density of 180 f.u. (Sec. II-C). Members of the sample are denoted by the symbol † in Table V, Column 1.

The 178-MHz sample has been selected from the Revised 3C Catalogue (Bennett 1962) with flux densities revised as noted in Sec. III. It contains 75 sources in the region $\delta>-5°$, $|b|>15°$ whose revised 178-MHz flux densities exceed 18.5 f.u. The source DA 240 (Galt and Kennedy 1968, Bridle, Davis, Fomalont, and Lequeux 1972a) has been added and the galactic source 3C 363.1 has been excluded. Members of this sample are denoted by * in Column 1 of Table V.

TABLE VI. Spectral indices of sources in the high-frequency samples.

Source	Id	Spectral class	α_{70}	α_{200}	α_{600}	α_{1800}
3C 48	Q	C−	0.1	0.47	0.69	0.83
CTA 21 (0316+16)	□	C−		−0.4	−0.1	0.55
3C 272.1 [M84]	G	S		0.63		
4C 32.44 (1324+32)		Cx	0.8	0.0	0.2	0.46
3C 287	Q	C−	(−0.2)	0.3	0.52	0.58
4C 12.50 (1345+12)	G	C−		−0.9	0.1	0.44
4C 62.22 (1357+62)		C−		−0.6	−0.2	0.4
4C 10.39, P1414+11	G	Cx	0.57	0.51	0.51	0.69
P 0418+04.7		C−		−1.0	−0.5	0.62
CTD 93 (1607+26)		C−			−0.8	0.64
3C 343		C−	(0.0)	0.2	0.54	0.91
3C 343.1		C−	(0.1)	0.3	0.54	1.00
3C 345	Q	Cx		0.2	0.33	0.31
CTA 102 (2229+11)	Q	C−		−0.1	0.1	0.31
3C 454.3	Q	C+	0.35	0.29	0.23	0.06

TABLE XIV (*continued*)

(1)	(2)	(3)	(4)	(5)	(6)	(7)
		Spectral components				
				MHz		
Source	Spectrum	Class	Index	ν_m	ν_{eq}	Structural information
3C 84	Cx	...	...	...		Separation into spectral components difficult because of confusion with 3C 83.1 and unknown contribution of component 3C 84B (Ryle and Windram 1968) at various frequencies. Steep low-frequency component usually associated with 3C 84A(iii) (Ryle *et al.* 1968) of size 5′ to 8′.5 (F1, CH, L) roughly coincident with envelope of filaments of NGC 1275. May have index as high as 2.0. BC—Significant cluster association.
3C 98	Cx	C_L−	0.95	15	1000	M—Double; preceding component has higher index. Tabulated fit consistent with Mackay's components.
		S	0.45			
P0405–12	C+	S	1.15	...	1000	Ekers (1969)—0′.5 NS×<0′.4 EW. F1—<15″ EW. No supporting evidence of components.
		S	0.15	...		
3C 111	Cx	C_L−	0.90	10	2300	M—Three major components; outer ones with steeper spectra. Tabulated fit consistent with Mackay's components, outer ones 9 f.u. inner ones 5.6 f.u. at 1.4 GHz. Turnover probably due to interstellar free–free absorption (b=−9°).
		S	0.20	...		
3C 131	Cx	S	2.5	...	20	F1—Unresolved, <15″ EW HH—IPS 20% implies structure <0″.2 at 400 MHz. No supporting evidence for components. Two fits represent extremes of possible two-component combinations.
		C_H−	0.75	...		
	Cx	S	1.7	...	95	Second fit consistent with self-absorption of small-diameter component.
		C−	...	90		
3C 135.1	C+	S	1.1	...	200	CH—Diameter >10″ No supporting evidence for components.
		S	0.5	...		
3C 144	C_L+	C_L−	2.5	...	16	Cronyn (1970)—Low-frequency component may be integrated emission from pulsar 0532. Fit assumes correction for interstellar absorption: $\tau \approx 0.75$ at 10 MHz.
		C_L−	0.25	25		
3C 166	Cx	C_L−	1.2	≤27	680	Elsmore and Mackay (1969)—Not resolved; <9″×<13″. HH—IPS 20% indicates some structure <0″.5 Turnover due to either self absorption or interstellar absorption (b=8°).
		S	0.40	...		
3C 198	Cx	C_L−	2.1	<10	65	F2—Double with components 1′.3 and 1′.5 diameter, separated 3′.5 at 1.4 GHz. HH—IPS <20% at 430 MHz. Caswell *et al.* (1967) 178-MHz map shows south extension to source. Tabulated fit lacks supporting evidence. Two-component fit difficult.
		C_L−	1.8	~90	600	
		C_L−	1.2	~700		
4C 55.16	Cx	S	0.7	...	350	No supporting evidence for components.
		C−	...	1500		

TABLE XIV (*continued*)

(1)	(2)	(3)	(4)	(5)	(6)	(7)
		Spectral components		MHz		
Source	Spectrum	Class	Index	ν_m	ν_{eq}	Structural information
P0832+14	Cx	S	1.5	...	130	HH—IPS <20% at 430 MHz.
		C_L-	1.5	150		
4C 29.31	C+	S	1.4	...	450	HH—IPS <40%.
		S	0.3	...		No supporting evidence of components.
P0854+09	C+	S	3.0	...	16	HH—IPS<20%.
		S	0.95	...		No supporting evidence for low-frequency component which depends on 10 MHz measure only.
3C 216	Cx	C_L-	0.90	16	8000	B—Gaussian source 2".6 diameter.
		S	~0.0	...		LH-IPS. Model I 2" diameter source; Model II 20% less than 0".7.
						No supporting evidence for flat-spectrum high-frequency component.
3C 247	Cx	S	1.2	...	100	Mitton (1970)—Double, each component <(5"×3").
		C_L-	0.88	170		BB—50% of source in component 0".7 diameter, possibly associated with high-frequency (C_L-) component.
						F1—Core/halo. Halo 3'.3 diameter, may be low-frequency component.
3C 264	Cx	C_L-	3.0	<12	20	MKN—Source 220"×100" at 408 MHz is 2.6 times larger in solid angle than at 1407 MHz. Up to 20% of flux density at 408 MHz may be in extended components not shown on map: low frequency component would not exceed this.
		S	0.78	...		RCL—Emission at 22 MHz may be from broad region (~40').
						BC—significant association with cluster.
3C 273	Cx	S	1.75	...	42	Hazard, Gulkis, and Bray (1966)—Occultations at several frequencies favor low-frequency source nearer position of 3C 273B than 3C 273A.
		C_L-	0.63	40	1000	Slee and Wraith (1967)—38-MHz interferometry shows 130 f.u. (~50%) within 3" diameter.
		C−	<0.0	...		Proposed fit consistent with a separate low-frequency source near 3C 273B of angular diameter >3".
3C 286	Cx	S	0.75	...	100	BB—IPS indicates 90% of source within 0".7 diameter.
		C_L-	0.47	300		Clarke *et al.* (1969)—Model at 400 MHz: 10% <0".005, 60% (0".05×0".03), 30% (0".03×7".2) at p.a. 38°.
						Third component in Clarke's model, extended in one direction, could dominate at low frequencies.
3C 287	Cx	S	1.05	...	270	F1, F2—Displaced core/halo model A<18", 1.4 f.u.; B ~2'.1, 1.5 f.u.; separation 1'.2 EW
		S	0.50	...		LH, HH—IPS <20% at 80 and 430 MHz.
	Cx	S	0.95	...	1700	Second fit is to Fomalont's components.
		C−	...	1300		

TABLE XIV (*continued*)

(1)	(2)	(3)	(4)	(5)	(6)	(7)
		Spectral components		MHz		
Source	Spectrum	Class	Index	ν_m	ν_{eq}	Structural information
3C 293	[1]Cx	S	≤1.1	···	100–500	M. Branson *et al.* (1972)—Maps at 1.4, 2.7, and 5 GHz show main component, faint outer components and separate preceding component. Outer component may provide low frequency excess. F1, F2—Displaced core/halo. Spectral components poorly defined.
		C−	···	<400		
3C 298	[1]Cx	S	1.7	···	60	BB—IPS indicates 70% of source within 0″.8 diameter at 80 MHz. Fit consistent with this being C_L− component. Anderson and Donaldson (1967)—Double, components 0″.5 separated by 1″.2. HH—IPS 50%.
		C_L−	1.10	100		
3C 334	Cx	C_L−	1.8	29	180	MKN—Map shows a double source with perhaps a bridge and outlying emission. B—Wide double with equal components accounts for 40% of flux density. HH—IPS <20%. Fitted components do not correspond to double structure given by MKN.
		C−	(0.5)	150		
3C 380	Cx	C_L−	0.90	19	2400	B—single guassian source 2″.1 diameter. Donaldson et al. (1969)—At 1420 MHz 43% is <0″.10; at 2690 MHz 50% <0″.025. Clark *et al.* (1968)—50% <0″.03 at 1660 MHz.
		(S)	0.15	···		
3C 402	Cx	S	1.4	···	130	MKN—Map shows complex region. Fit to total spectrum indicates ≥70% of flux density near 20 MHz comes from most northerly component of MKN (cf RCL).
		C−	···	<100		
3C 430	Cx	C_L−	1.4	≤15	25	MKN—Map shows two peaks and surrounding emission. F1—Diameter ~40″ EW. Low-frequency component possibly associated with outlying emission. Turnover possibly due to interstellar free–free absorption (b=8°).
		C_L−	0.68	≤15		
3C 445	C+	S	1.4	···	40	L—Map at 80 MHz shows source ~(12′ ×5′) at p.a. 150°. F1—Double with components 40″ separated 1′ EW.
		S	0.70	···		
3C 446	C+	S	1.3	···	80	B—Double, unresolved components 15″ apart, flux density ratio 16:1. Donaldson *et al.* (1971)—Core/halo; core <0″.04, halo 0″.4 EW×0″.2 NS. Clark *et al.* (1968)—50% flux density in component <0″.04. Clarke *et al.* (1969)—diameter 0″.034 at 430 MHz.
		S	0.35	···		
3C 454.2	C+	S	≤2.0	···	50	F1—Unresolved, <15″. High-frequency component may be curved (C−).
		(S)	0.75	···		

Notes to TABLE XIV.

[1] Indicates spectrum classification is not the primary one for this source in Table V.

Abbreviations used in Column 7.

A Allen *et al.* (1962) 158 MHz 2200λ–6100λ interferometer.
B Bash (1968) 2695 MHz. 10000λ–24000λ interferometer.
BB Burnell (1972) IPS 81.5 MHz.
BC Bridle and Costain (in preparation).
CH Clark and Hogg (1966) 2695 MHz 21500λ interferometer.
F1 Fomalont (1968) 1425 MHz. 144λ–2626λ east-west interferometer.
F2 Fomalont (1971) 1425 MHz. 144λ–2626λ E–W, N–S interferometer.
HH Harris and Hardeback (1969) IPS. 430 MHz.
L Lockhart (1971) 80 MHz 3′.8 pencil beam.
LH Little and Hewish (1968) IPS. 178 MHz.
M Mackay (1969) 408 MHz. 1407 MHz. Resolution 20″.
MKN Macdonald *et al.* (1968) 408 MHz, 1407 MHz. Resolution 20″.
RCL Roger *et al.* (1969).

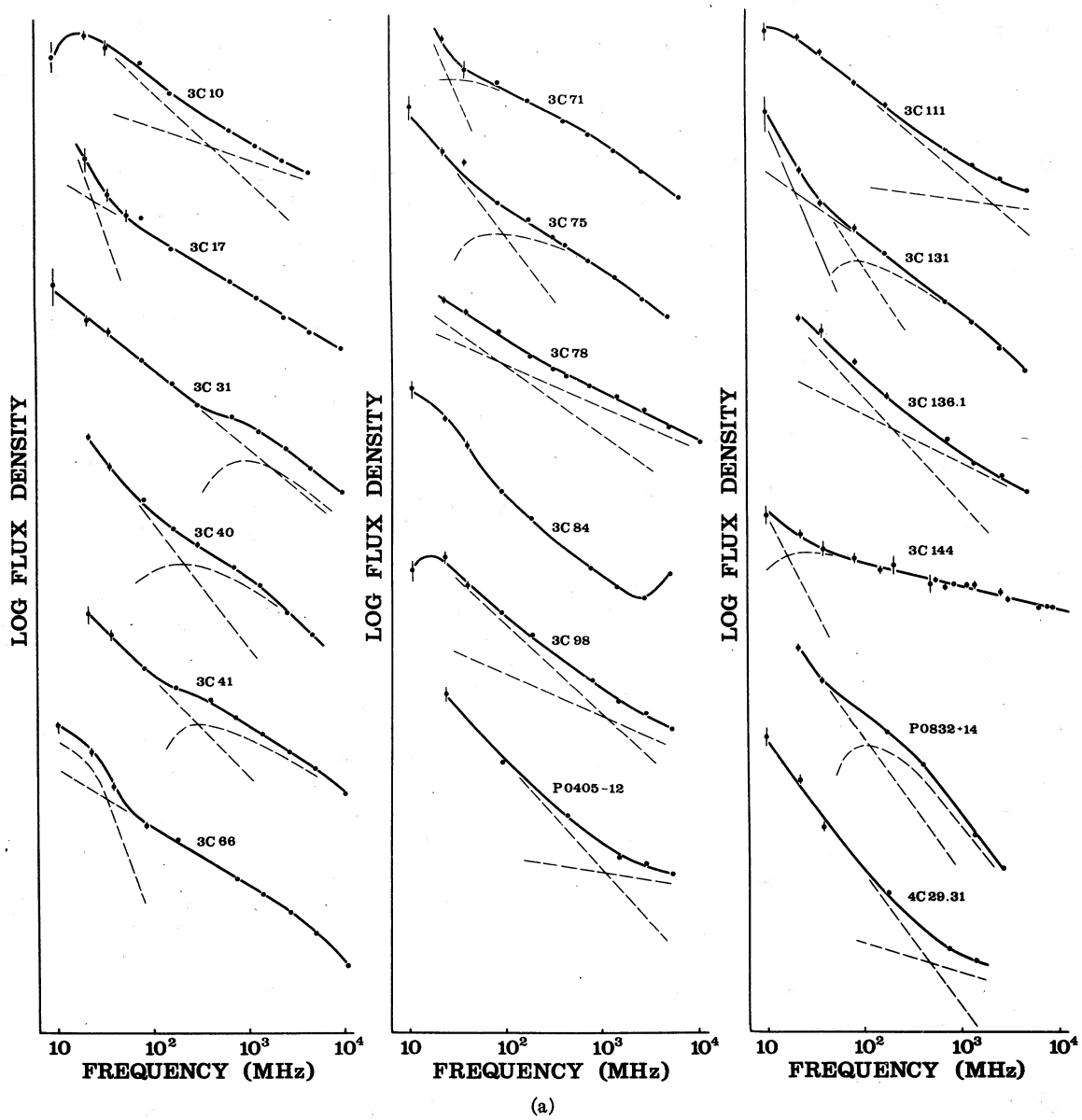

(a)

FIG. 6 (a–b). The spectra of radio sources with some evidence of positive curvature. Dashed lines indicate possible spectral components which could account for the observed total spectrum. The reality of these components is assessed in Table XIV.

and 5% levels of confidence for coefficients of 0.42 and 0.33, respectivelv. The correlation between luminosity and spectral index is therefore statistically significant, whereas those between emissivity and index or volume and index are not.

It is necessary to consider whether or not the correlations of emissivity and volume with spectral index could appear insignificant simply because of uncertainties in the angular sizes used to calculate these parameters. To test this, angular sizes for 14 sources given both by Fomalont (1968) and by Macdonald *et al.* (1968) were used separately to calculate emissivity and volume. The rms difference between the corresponding pairs of values permits estimation of the intrinsic dispersion in these parameters. If there were a high correlation between emissivity (or volume) and spectral index, the intrinsic dispersion is sufficient to reduce any correlation coefficient between luminosity and spectral index to less than about 0.3. Since this is much lower than the value actually calculated we must conclude that the luminosity–spectral index relation is the significant one.

Inclusion of the spectral indices of the N and db galaxies does not significantly alter the correlations. The QSS are in two groupings, the most numerous having average volume and high emissivity and the

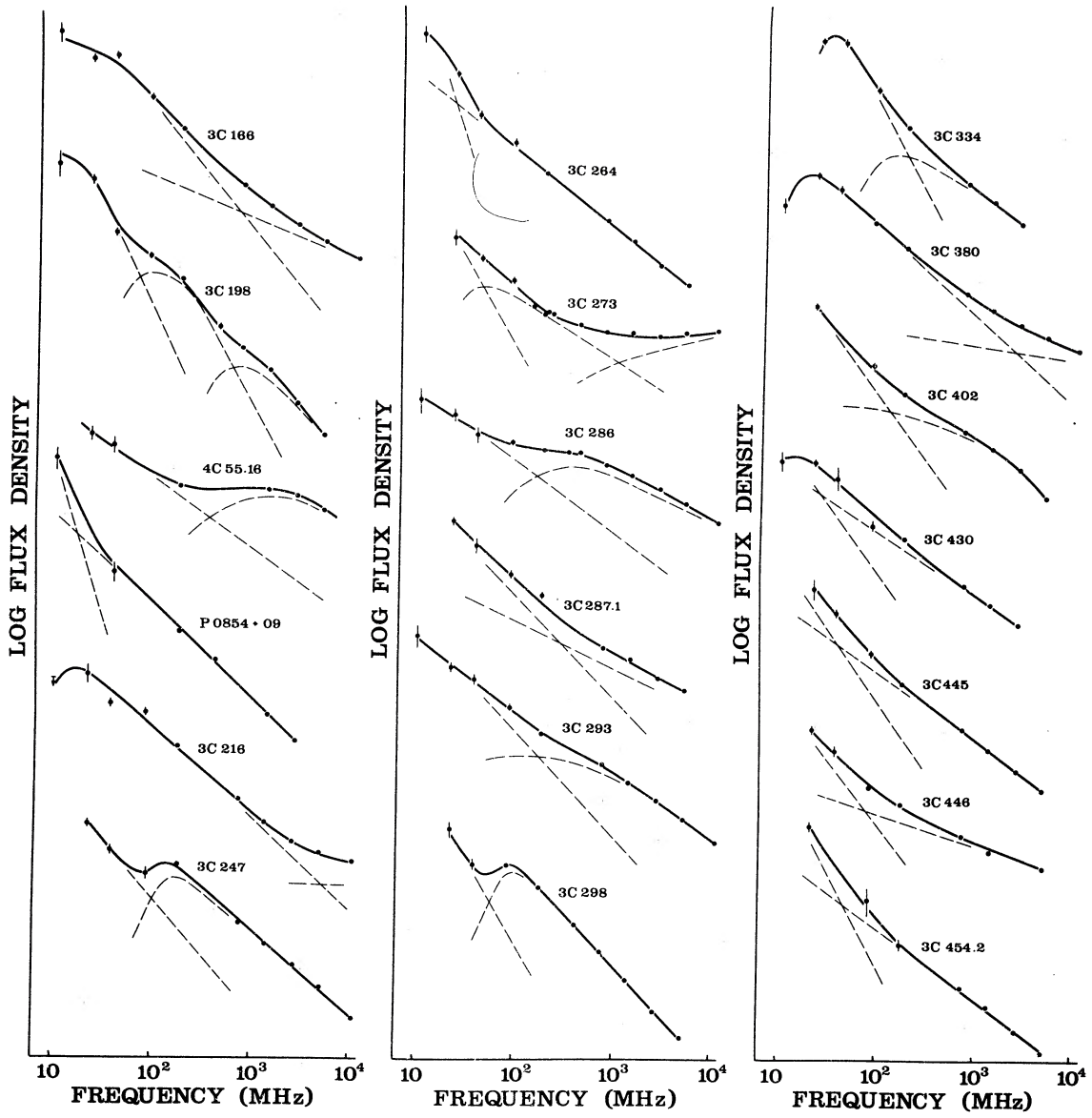

(b)

FIG. 6 (*continued*)

other with large volume and less than average emissivity. All have high luminosity. The median spectral index for the transparent QSS is 0.98, considerably in excess of the median for ordinary radio galaxies.

Bridle *et al.* noted that the distribution of luminosities in their sample is determined almost entirely by the distribution of redshifts (or apparent magnitudes) since the range in flux density for the sample is small. This is equally true with the present galaxy sample; if one correlates spectral index with apparent magnitude, the correlation coefficient is virtually the same as that between index and luminosity. In this context it is of interest to consider the distribution of transparent spectral indices for sources in blank fields. If, as is often assumed, these sources are mostly radio galaxies at great distances, then they will be sources of high-radio luminosity and should have a distribution of spectral indices consistent with the derived trend. Figure 5 shows the spectral-index distributions for the blank field sources, for radio galaxies with apparent magnitudes greater and less than 17.5 and for the QSS. The distribution for blank field sources least resembles that of the QSS and a χ^2 test indicates less than 1% probability that the blank field sources are a random selection from a population whose spectral indices are distributed like those of the QSS. A similar test reveals

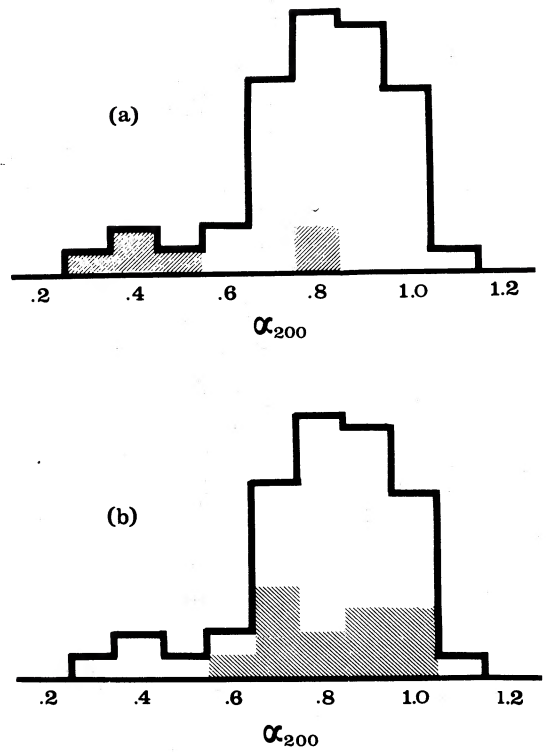

FIG. 7. Distribution of the spectral indices at 200 MHz for radio sources at galactic latitudes $|b|<15°$. The shaded areas represent (a) supernova remnants and (b) optically obscured sources.

less than a 5% chance that the blank fields are entirely a random selection from the population of optically faint radio galaxies. The blank fields are therefore unlikely, from the evidence of their spectra, to contain many quasistellar objects, but are also unlikely to be entirely high-luminosity radio galaxies. Indeed, the spectral data of these small samples would suggest that the blank fields are most similar to the radio galaxies as a whole (i.e., both high- and low-luminosity).

B. Multicomponent Sources

Sources exhibiting some positive curvature in their total spectra are classified as $C+$, C_L+, and Cx in Table V. In most cases these are likely to have two or more distinct components with significantly different spectral properties.

Table XIV contains an analysis of these spectra. In each case the spectrum below 2 GHz has been split into two (occasionally three) plausible components each with a spectral class as indicated in Column three. Here the classification C_L- and C_H- refer to curvature confined to the low or high frequency extreme appropriate for the source components only. Column 4 lists the spectral index for power-law sections of the component spectra. Column 5 gives the frequencies of maximum flux density for components showing turnovers. Column 6 is a list of the frequencies at which the proposed components contribute equally to the flux density. Structure revealed by high-resolution pencil-beam and interferometer studies of these sources and by interplanetary scintillation observations which may relate to the identification of the spectral components are noted in Column 7. The total spectra and the suggested components are illustrated in Fig. 6. It must be emphasized that in proposing these "plausible components" we do not wish, unless there is supporting evidence, to imply that the separation proposed is unique. The table is intended to draw attention to the possible range of complexity of the low-frequency spectra.

There are several difficulties which hinder attempts to associate spectral components with structure revealed by higher frequency measurements of high resolution. First, it is easily shown, that, even under favorable conditions, two power-law spectral components must have indices differing by at least 0.3 before curvature in the total spectrum is detectable with present day measurement errors (Bridle 1969). An example of such a spectrum is that of 3C 78 in which the complex fit shown in Fig. 6 is listed as a second preference in Table V. A second difficulty is that components with high spectral indices which produce excess flux density at low frequencies are often too weak or of too low surface brightness to appear in high-resolution maps at shorter wavelengths (e.g., 3C 66). Only greatly improved resolution at long wavelengths or sensitivity at short wavelengths can be expected to reveal details of such structure. The low resolution of the low-frequency observations also makes it difficult to rule out the possibility that excess flux density apparent in a total spectrum is due to a physically unrelated (confusing) source (e.g., 3C 75). The presence of nearby small-diameter sources can often be checked by reference to high-sensitivity surveys at higher frequencies, but large diameter features partially or completely resolved by these surveys present a problem.

In many radio sources in Table XIV structure covering a wide range of angular diameters has been measured. The steeper spectrum low-frequency components are usually associated with the more extended emission or halos. 3C 40, 3C 66, 3C 247, 3C 265, 3C 273, 3C 286, and 3C 430 are examples of this. In some cases the association is merely one of default, because the flatter spectral component (if there are two) which becomes optically thick and disappears at long wavelengths most likely corresponds to the structure of small angular size if self-absorption is operative. Nevertheless, some radio sources do appear to have extended components with high-spectral indices; such components may represent fossil remnants of powerful initial outbursts in which E^2 losses (e.g., synchrotron losses, inverse Compton losses) or differential diffusion have preferentially depleted the higher energy electrons.

C. The Spectra of Sources at Low Galactic Latitudes

The spectra of radio sources close to the galactic plane require separate consideration for several reasons; firstly, because any sample at low latitudes will contain galactic sources, supernova remnants (SNR) in particular, and secondly, because at low frequencies the effects of free–free absorption by interstellar ionization can be expected. Furthermore, obscuration precludes optical identification of many sources at low latitudes.

Of the 47 sources listed in Table V for which $|b|<15°$, 13 are obscured. Six sources are identified with SNR's. The remaining 18 identified sources contain radio galaxies and QSS's in a proportion similar to that found at higher latitudes. The distribution of the spectral indices at 200 MHz for the 47 sources is shown in Fig. 7, with shading to indicate the indices of the SNR's and obscured sources. It can be seen that whereas the SNR's have distinctly flatter spectra on average, the obscured sources have indices evenly displaced about the median. Hence, purely on grounds of spectral index one would suspect that the obscured sources are mostly extragalactic.

The 41 sources other than the SNR's have only 30% of their spectra classified as straight compared to 41% for samples of sources with $|b|>15°$: the difference is made up by spectra with negative curvature, probably due to free–free absorption. In all, 19 of the low-latitude sources have spectral curvature at low frequencies which might be attributed to interstellar absorption. These are indicated as FFA in Column 12 of Table V together with an estimate of optical depth implied by a fit to the spectral curvature. The effect is apparent on slightly more than half the sources at $|b|\leq 5°$ and on about one-third of those with range $5°<|b|<15°$.

VII. CONCLUSIONS

We have considered radio source spectra extended by new measurements at the lowest available frequencies. In interpreting the spectral properties of radio sources, it is essential to consider separately the range of the spectrum displaying negative curvature and that showing a power-law variation. Only in this latter range, if the source is transparent, can the spectral index reflect the electron energy spectrum.

A. Power-law Spectra

It is now well established that radio galaxies with power-law spectra have spectral indices which correlate with the total radio luminosities of the galaxies. This effect appears to be largely independent of any evolutionary expansion of the sources. However, samples of identified sources reaching at least an order of magnitude weaker in flux density will be required to distinguish index–redshift (or index–apparent magnitude) correlation from index–luminosity correlations.

If one assumes that the redshifts of quasistellar sources indicate their distances, then these are among the most luminous of radio sources and the transparent indices are correspondingly high. It is, however, only on the basis of redshift determined distances that the majority of QSS can be classed as having high radio luminosity. Hence, whether or not the same physical process which links radio galaxy luminosity and the electron energy spectrum is also operative in QSS hinges on the interpretation of QSS redshifts.

The nature of some sources identified with blank fields is also in question since several in a small sample show power-law spectral indices characteristic of neither high-luminosity radio galaxies nor QSS. The distribution of spectral indices for the blank field sources most resembles that of radio galaxies as a whole. Spectral indices for a larger sample may clarify the nature of these blank fields.

B. Absorption Effects in Total Spectra

The proportion of "turnover" spectra for sources at latitudes $|b|<15°$ is greater than that at higher latitudes. Hence the presence of interstellar absorption is statistically confirmed. However, even for latitudes $|b|<5°$ by no means all extragalactic sources exhibit spectral curvature at 20 MHz.

At higher latitudes a large fraction of radio sources with unusually low spectral indices are known from interplanetary scintillation measurements to have compact structure. Conversely, most sources which exhibit IPS have spectral curvature at low frequencies. QSS comprise a large proportion of both groups. Amongst the scintillators the spectral curvature is more pronounced the greater the degree of scintillation and is likely due to synchrotron self-absorption. The spectral class C_L- contains a large proportion of QSS and it is probably for this reason that the median index for the class is higher than that of the S class. On the other hand, the nonscintillators are mostly radio galaxies and power-law spectra predominate. One can conclude, then, that the division of radio sources into radio galaxies and QSS is supported to some extent by their radio spectra.

It is noteworthy that few sources with self-absorption curvature have spectra with well-measured opaque portions of index near -2.5 such as that measured for PKS 1934–63 (Kellermann 1966b). There are probably two reasons for this. First, such a total spectrum will occur only when the source has a well-defined boundary and contains no other lower frequency components. Second, even when this condition is met, with present day measurements at discrete well-spaced frequencies, there is a good chance that the flux density may be measured easily near the turnover frequency but lie below the sensitivity limit at the next lower discrete frequency. 3C 275.1 is an example of this.

TABLE XV. Suggested calibration sources.

Source	20 MHz Flux density $10^{-26} W m^{-2} Hz^{-1}$	Spectral index	Power-law Range Lower	Upper
3C 33	290	0.72	10 MHz	6 GHz
3C 161	210	0.67	20	1
3C 196.1	250	1.16	20	6
3C 205	90	0.88	10	1
3C 218	2450	0.97	20	6
3C 270	230	0.61	20	6
3C 274	6150	0.80	10	6
3C 280	135	0.80	10	1
3C 348	3350	1.01	10	6
3C 353	1230	0.73	10	6

VIII. CALIBRATION SOURCES FOR FUTURE MEASUREMENTS

Because of differences in the flux density scales discussed in Sec. II, only half of the 161 sources considered, both in the present study and in that of Braude *et al.* (1970b) are classified in the same way. As one might expect, the discrepancies are predominantly in the sense that Braude *et al.* find a larger proportion of radio sources with positive curvature in their spectra and fewer with negative curvature. Individual differences are too numerous to cite.

In general, agreement of the two scales is confined to sources stronger than 1000 f.u. near 20 MHz. In particular, however, there are a number of weaker sources whose spectra even to 10 MHz agree in the two studies. Table XV contains a list of ten sources, all with power-law spectra at low frequencies for which there is good agreement both in flux density and in spectral index. We suggest that these be included as calibration sources in future observations.

ACKNOWLEDGMENTS

We are indebted to Dr. W. C. Erikson, Dr. M. Viner, Professor S. Ya. Braude, Dr. J. R. Shakeshaft, Dr. A. Niell, and Dr. J. J. Condon for providing us with their measurements prior to publication.

REFERENCES

Abell, G. O. (1958). Astrophys. J. Suppl. Ser. **3,** 211.
Allen, L. R., Anderson, B., Conway, R. G., and Palmer, H. P. (1962). Mon. Not. R. Astron. Soc. **124,** 477.
Anderson, B., and Donaldson, W. (1967). Mon. Not. R. Astron. Soc. **137,** 81.
Andrew, B. H. (1967). Astrophys. J. **147,** 423.
Artyukh, V. S., Vitkevich, V. V., Dagkesamanskii, R. D., and Kozhukhov, V. N. (1969). Sov. Astron.-AJ **12,** 567.
Bash, F. N. (1968). Astrophys. J. Suppl. Ser. **16,** 373.
Bennett, A. S. (1962). Mem. R. Astron. Soc. **68,** 163.
Bozyan, E. P. (1968). Astrophys. J. **157,** L77.
Branson, N. J. B. A., Elsmore, B., Pooley, G. G., Ryle, M. (1972). Mon. Not. R. Astron. Soc. **156,** 377.
Braude, S. Ya., Lebedeva, O. M., Megn, A. V., Ryabov, B. P., and Zhouck, I. N. (1969). Mon. Not. R. Astron. Soc. **143,** 289.
Braude, S. Ya., Lebedeva, P. M., Megn, A. V., Ryabov, B. P., and Zhouck, I. N. (1970a). Astrophys. Lett. **5,** 129.
Braude, S. Ya., Megn, A. V., Ryabov, B. P., and Zhouck, I. N. (1970b). Astrophys. Space Sci. **8,** 275.
Bridle, A. H., and Purton, C. R. (1968). Astron. J. **73,** 717.
Bridle, A. H. (1967). Observatory **87,** 60.
Bridle, A. H. (1968). J. Roy. Astron. Soc. Canada **62,** 193.
Bridle, A. H. (1969). Nature (Lond.) **224,** 889.
Bridle, A. H., and Costain, C. H. (1970). J. Roy. Astron. Soc. Canada **64,** 184.
Bridle, A. H., and Davis, M. M. (1973). Personal Communication.
Bridle, A. H., Davis, M. M., Fomalont, E. B., and Lequeux, J. (1972). Astron. J. **77,** 405.
Bridle, A. H., and Feldman, P. A. (1972). Nat. Phys. Sci. **235,** 168.
Bridle, A. H., Kesteven, M. J. L., and Guindon, B. (1972). Astrophys. Lett. **11,** 27.
Burnell, S. J. (1972). Astron. Astrophys. **16,** 379.
Caswell, J. L., and Crowther, J. H. (1969). Mon. Not. R. Astron. Soc. **145,** 181.
Caswell, J. L., Crowther, J. H., and Holden, D. J. (1967). Mem. R. Astron. Soc. **72,** 1.
Clark, B. G., and Hogg, D. E. (1966). Astrophys. J. **145,** 21.
Clark, B. G., Kellermann, K. I., Bare, C. C., Cohen, M. H., and Jauncey, D. L. (1968). Astrophys. J. **153,** 705.
Clark, T. A. (1966). Astron. J. **71,** 158(A).
Clarke, R. W., Broten, N. W., Legg, T. H., Locke, J. L., and Yen, J. L. (1969). Mon. Not. R. Astron. Soc. **146,** 381.
Condon, J. J. (1971). Personal communication.
Conway, R. G., Kellermann, K. I., and Long, R. J. (1963). Mon. Not. R. Astron. Soc. **125,** 261.
Costain, C. H., Bridle, A. H., and Feldman, P. A. (1972). Astrophys. J. **175,** L15.
Costain, C. H., Lacey, J. D., and Roger, R. S. (1969). IEEE Trans. Antennas Propag. **AP-17,** 162.
Cronyn, W. M. (1970). Science **168,** 1453.
Doherty, L. H., MacLeod, J. M., and Purton, C. R. (1969). Astron. J. **74,** 827.
Donaldson, W., Miley, G. K., Palmer, H. P., and Smith, H. (1971). Mon. Not. R. Astron. Soc. **146,** 213.
Ekers, R. D. (1965). Aust. J. Phys. Astrophys. Suppl. No. 6.
Ellis, G. R. A., and Hamilton, P. A. (1966). Astrophys. J. **143,** 227.
Elsmore, B., and Mackay, C. D..(1969). Mon. Not. R. Astron. Soc. **145,** 361.
Fomalont, E. B. (1968). Astrophys. J. Suppl. Ser. **15,** 203.
Fomalont, E. B. (1971). Astron. J. **76,** 513.
Galt, J. A., and Kennedy, J. E. D. (1968). Astron. J. **73,** 135.
Galt, J. A., Purton, C. R., and Scheuer, P. A. G. (1967). Publ. Dom. Obs. Can. **25,** 295.
Gower, J. F. R., Scott, P. F., and Wills, D. (1967). Mem. R. Astron. Soc. **71,** 49.

Hamilton, P. A., and Haynes, R. F. (1968). Aust. J. Phys. **21,** 895.
Harris, D. E., and Hardebeck, E. G. (1969). Astrophys. J. Suppl. Ser. **19,** 115.
Hazard, C., Gulkis, S., and Bray, A. D. (1966). Nature (Lond.) **212,** 461.
Heeschen, D. S. (1960). Publ. Astron. Soc. Pac. **72,** 368.
Howard, W. E., and Maran, S. P. (1965). Astrophys. J. Suppl. Ser. **10,** 1.
Kellermann, K. I. (1964). Astrophys. J. **140,** 969.
Kellerman, K. I. (1966a). Astrophys. J. **148,** 621.
Kellerman, K. I. (1966b). Aust. J. Phys. **19,** 195.
Kellermann, K. I. (1966b). **19,** 195. .
Kellermann, K. I., and Pauliny-Toth, I. I. K. (1971). Astrophys. Lett. **8,** 153.
Kellermann, K. I., Pauliny-Toth, I. I. K., and Williams, P. J. S. (1969). Astrophys. J. **157,** 1.
Kenderdine, S. (1963). Mon. Not. R. Astron. Soc. **126,** 55.
Little, A. G. (1958). Aust. J. Phys. **11,** 70.
Little, L. T., and Hewish, A. (1966). Mon. Not. R. Astron. Soc. **134,** 221.
Lockhart, I. (1971). Ph.D. thesis, Australian National University, Canberra.
Macdonald, G. H., Kenderdine, S., and Neville, A. C. (1968). Mon. Not. R. Astron. Soc. **138,** 259.
Mackay, C. D. (1969). Mon. Not. R. Astron. Soc. **145,** 31.
MacLeod, J. M., and Doherty, L. H. (1972). Nature (Lond.) **238,** 89.
Mills, B. Y., Slee, O. B., and Hill, E. R. (1958). Aust. J. Phys. **11,** 360.
Mitton, S. (1970). Mon. Not. R. Astron. Soc. **149,** 101.
Moffet, A. T., Schmidt, M., Slater, C. H., and Thompson, A. R. (1967). Astrophys. J. **148,** 283.
Munro, R. E. B. (1971). Aust. J. Phys. **24,** 743.
Niell, A. (1971). Personal communication.
Olsen, E. T. (1967). Astron. J. **72,** 738.
Parker, E. A. (1968). Mon. Not. R. Astron. Soc. **138,** 407.
Pauliny-Toth, I. I. K., Wade, C. M., and Heeschen, D. S. (1966). Astrophys. J. Suppl. Ser. **13,** 65.
Pilkington, J. D. H., and Scott, P. F. (1965). Mem. R. Astron. Soc. **69,** 183.
Roub, G. (1969). Publ. Univ. Bologna, Contrib. 55.
Ryle, M. and Longair, M. S. (1967). Mon. Not. R. Astron. Soc. **136,** 123.
Ryle, M., and Windram, M. D. (1968). Mon. Not. R. Astron. Soc. **138,** 1.
Scott, P. F., and Shakeshaft, J. R. (1971). Mon. Not. R. Astron. Soc. **154,** 198.
Scheer, D. J., and Kraus, J. D. (1967). Astron. J. **72,** 536.
Schilizzi, R. T., Lockhardt, I. A., and Wall, J. V. (1972). Aust. J. Phys. **25,** 545.
Shimmins, A. J., and Day, G. A. (1968). Aust. J. Phys. **21,** 377.
Shlovskii, I. S. (1960). Sov. Astron.-AJ **4,** 243.
Slee, O. B. and Wraith, P. K. (1967). Nature (Lond.) **214,** 971.
Smith, M. A. (1968). Ph.D. thesis, University of Cambridge. Staff of Radiophysics Division, CSIRO, (1969). Aust. J. Phys. Astrophys. Suppl. 7.
van der Laan, H. (1969). Astron. Astrophys. **3,** 477.
Véron, M. P., Véron, P., and Witzel, A. (1972). Astron. Astrophys. **18,** 82.
Viner, M. (1971). personal communication.
Wall J. V., Shimmins, A. J., and Merkelijn, J. K. (1971). Aust. J. Phys. Astrophys. Suppl. 19.
Williams, P. J. S., and Bridle, A. H. (1967). Observatory **87,** 280.
Williams, P. J. S., Kenderdine, S., and Baldwin, J. E. (1966). Mem. R. Astron. Soc. **70,** 53.
Wills, D. (1966). Observatory **86,** 140.
Willson, M. A. G. (1970). Mon. Not. R. Astron. Soc. **151,** 1.
Zimmermann, P. (1970). Beiträge zur Radioastronomie **I,** 161.